



THE STUDY ON HIGH AND LOW-VOLTAGE MOSFETS

INTEGRATION ON InGaAs

Priyanka Malik¹, Pooja Devi², Nisha Malik³

¹Department of Physics, 1Bhagini Nivedita College, University of Delhi, Delhi, 110043, India

²Department of Physics, Shyamlal College, University of Delhi, Delhi, Delhi, 110032, India

³Department of Information Technology, University of Technology Sydney, Sydney, 2768, Australia

DOI: 10.6084/m9.figshare.22654915

ABSTRACT

Many electronic devices may benefit from higher performance and greater efficiency if high and low-voltage MOSFETs were integrated on InGaAs. Due to its better electrical characteristics compared to silicon, MOSFET integration on InGaAs has been a focus of study. MOSFETs are the most often utilized transistors in power electronics. More efficient and faster electronic devices for a wide range of uses might result from a deeper knowledge of the design, manufacturing, and characterization of both low and high-voltage MOSFETs on InGaAs, which is the focus of this research. This research investigates the integration of high- and low-voltage MOSFET on InGaAs.

Keywords: MOSFETs, InGaAs, transistors, power electronics, silicon.

1. INTRODUCTION

Smart PICs have been developed thanks to the combination of power stages with low-voltage analog and digital circuitry. The benefits of smart power ICs in modern electronic systems include reduced size, weight, and cost as well as enhanced performance and reliability; this is in addition to reduced power consumption and reduced interface functions. In addition, the development of low-power RFICs has been spurred by the rising expectations placed upon practical electronic systems.¹

Power consumption is cut down, isolation is increased, dependability is increased, and more small-signal analog or digital devices may be integrated with power devices, SOI technology is the technology of choice for these circuits. By reducing the MOSFET's physical dimensions, f_t and f_{max} have been attained up to many tens of GHz, making it suitable for use in small-signal applications despite its high current capacity and low capacitance. Power high voltage MOSFETs with breakdown voltages in the 30-80 V



range, on the other hand, see the extensive application in RF power integrated circuits.

To accommodate the gigahertz radio frequency signal, these devices typically have a gate length of 0.3 to 1.0 μm and a gate-oxide thickness of several tens of nanometers.²⁻³

Although silicon's excellent quality and thermodynamically SiO_2 have made it a popular choice for electronic device manufacturing, the performance of Si-based devices is reaching its limitations owing to features such as sluggish mobility. As a result, non-Si materials are required to boost the functionality of electronic devices, especially at high frequencies. Due to their improved transport capabilities, III-V based semiconductor materials have recently attracted a lot of interest from the scientific community.⁴⁻⁶

Over the last two decades, InGaAs has gained traction as a possible silicon replacement for use in cutting-edge, high-speed digital gadgets of the future. The lack of a readily available native oxide, analogous to silicon's SiO_2 , posed a significant challenge for InGaAs production. In the past, several attempts were made to perfect the InGaAs MOSFET production process by using better insulators.⁷⁻⁸

These studies prove that increased drive current, decreased access resistance, and enhanced transconductance may result from increased carrier mobilities and decreased effective masses. The investigation of InGaAs as a material for high-voltage power supplies was equally fascinating. Some findings in the literature show that power MOSFETs may benefit from high mobility InGaAs semiconductors in terms of improved performance (increased V_{br} , V_{br} is defined as the V_{DS} at which I_D is greater than 10×10^{-12} A/ μm , and I_D , decreased $R_{on,sp}$, greater g_m , better frequency responsiveness, and larger SOAs). Therefore, this chapter's goal is to investigate high- and low-voltage MOSFET integration on InGaAs. Smart power ICs on InGaAs will benefit from this idea.⁹⁻¹⁰

2. MATERIAL AND METHODS

2.1 DEVICE STRUCTURE

The combination of a low-voltage MOSFET with a junction-isolated high-voltage DTG MOSFET is shown in Fig. Both devices separate the drain contacts from the p-base and the source area with an oxide-filled trench and a vertical creation of n-channels in the p-base. At the same time, the current that drains flows in both directions, from the drain connection to the source contact. The oxide thickness plays a significant role in the extremely high voltage DTG

MOSFET. $t_{ox}=0.3 \mu\text{m}$, and $t_{ox1}=0.91 \mu\text{m}$, and $t_{ox2}=0.1 \mu\text{m}$. The length of a cell pitch is 3 meters, while the length of a gate is $0.5 \mu\text{micrometers}$; $L_1=0.6 \mu\text{m}$, $L_2=1.34 \mu\text{m}$, $L_3=0.46 \mu\text{m}$. Doping levels in the p-body are $8 \times 10^{16} \text{ cm}^{-3}$ and in the n-drift region are $1.5 \times 10^{16} \text{ cm}^{-3}$. Since the gates have more influence on ID when two channels are conducted through them at once, the ID and gm are improved. The high voltage DTG MOSFET has a greater ft and fmax when gm is large. Because of the improved RESURF effect, the drift area of a high-voltage DTG MOSFET is lengthened when it is folded in the horizontal and vertical directions, and the electric field is suppressed. This results in a greater V_{br} .

On top of the same InP substrate sits a layer of In_{0.53}Ga_{0.47}As with a doping concentration of $1 \times 10^{19} \text{ cm}^{-3}$, making up the low-voltage MOSFET. For ohmic source connections, we employ a 60 nm p-type In_{0.53}Ga_{0.47}As 95 layer with $2 \times 10^{18} \text{ cm}^{-3}$ of doping and a 20 nm In_{0.53}Ga_{0.47}As n -cap layer with $1 \times 10^{19} \text{ cm}^{-3}$ of doping layer, so reducing contact resistance by lowering the distance between the drain and the channel. The trench's Al₂O₃ blocks off the drain from the water supply. To keep the TaN gate electrode in place, a 2 nm-thick gate oxide is etched into a central trench. Improve gate control by shifting the SCEs by using a higher k dielectric material or reducing the oxide layer. If the gate potential in a vertical p-type InGaAs layer is increased over the threshold potential, then dual channels will form on both sides of the gate.

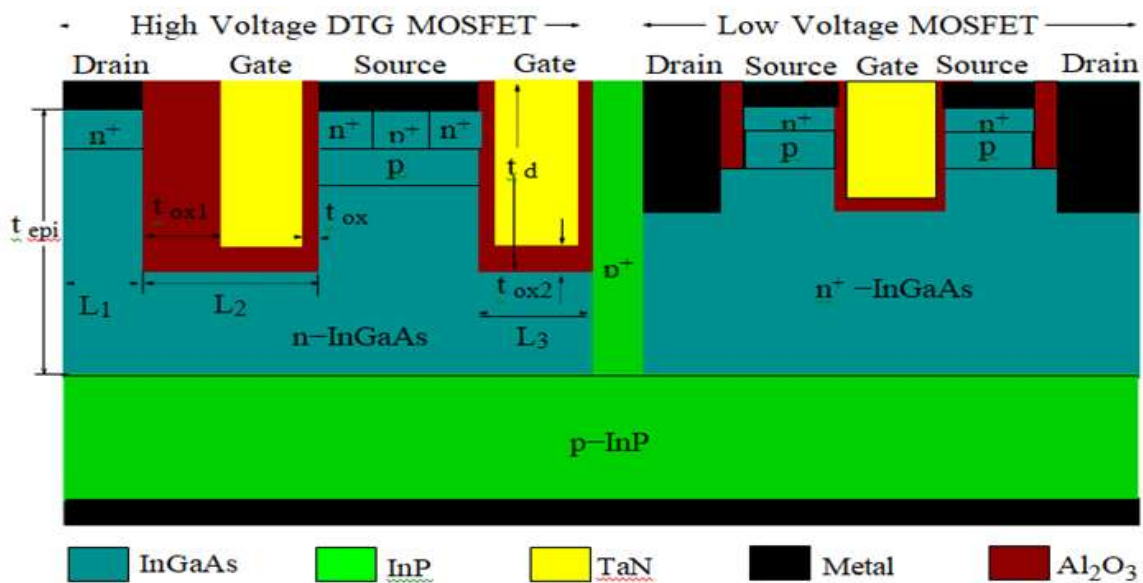
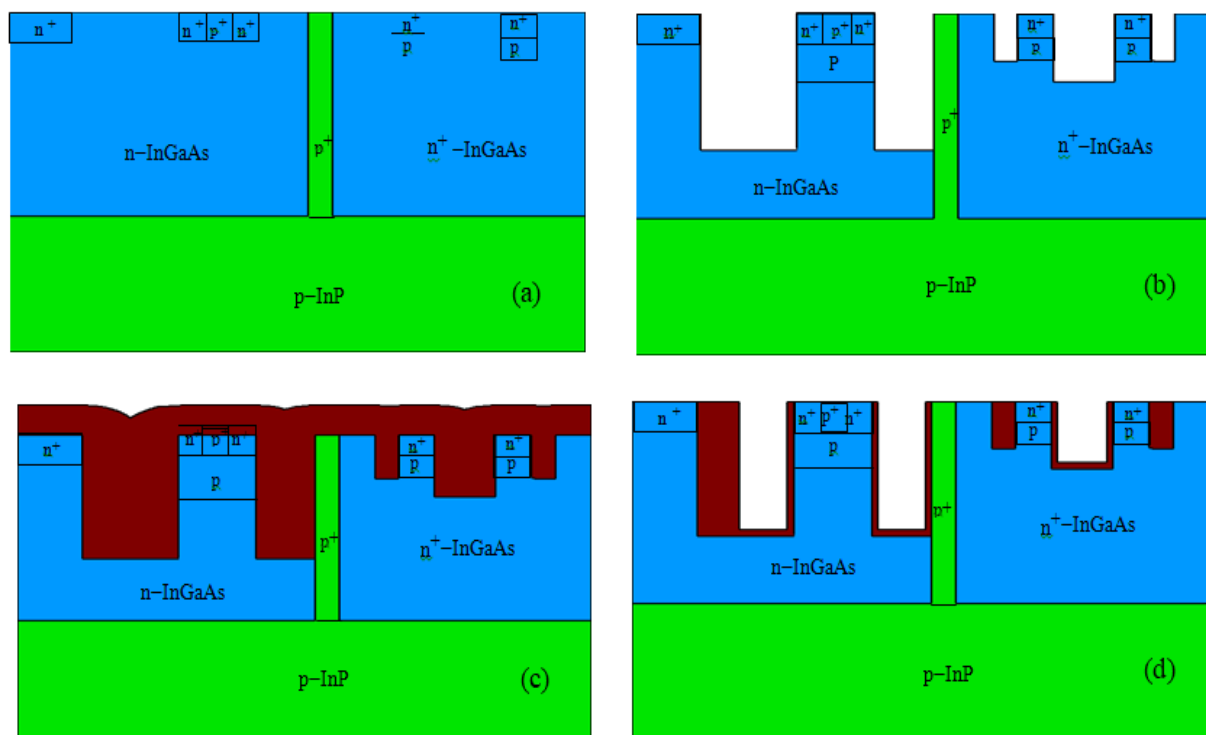


Figure1: The isolated junction cross section of a high-voltage DTG MOSFET with a low-voltage MOSFET.

The gm or ID are both increased by simultaneous channel conduction, leading to a higher ft and fmax. The recommended method of producing both high- and low-voltage MOSFETs with a junction isolation barrier is shown in Fig. ATHENA is used as a design tool for the fabrication process. “In this process, an n-InGaAs layer 2.2 μm thick is produced on top of an InP substrate with a doped concentration of $1.5 \times 10^{16} \text{ cm}^{-3}$. The implantation of boron and BF₂ results in p-base for both gadgets. The p or n zones are created by implanting ions of BF₂ and arsenic. As can be seen in Fig.1, the high-voltage DTG MOSFET is sandwiched between the lower-voltage MOSFET and a layer of heavily doped InP. For the high-voltage DTG MOSFET, two trenches are created using two separate masks; whereas for the low voltage MOSFET, three trenches are created using three separate masks (see Fig.2). As can be seen in Fig. Al₂O₃ completely coats the substrate. Al₂O₃ is etched away as indicated in Fig. in order to achieve a tox of 30 nm in a high-voltage DTG MOSFET and 2 nm in low voltage MOSFET.” In Fig.2, you can see how TaN completely coats the substrate. As can be seen in Fig., a field plate is carved out of TaN at the bottom of gate trenches. InGaAs surface etching is seen in Fig.2. The last step in creating isolated junction connections is metallization and patterning.



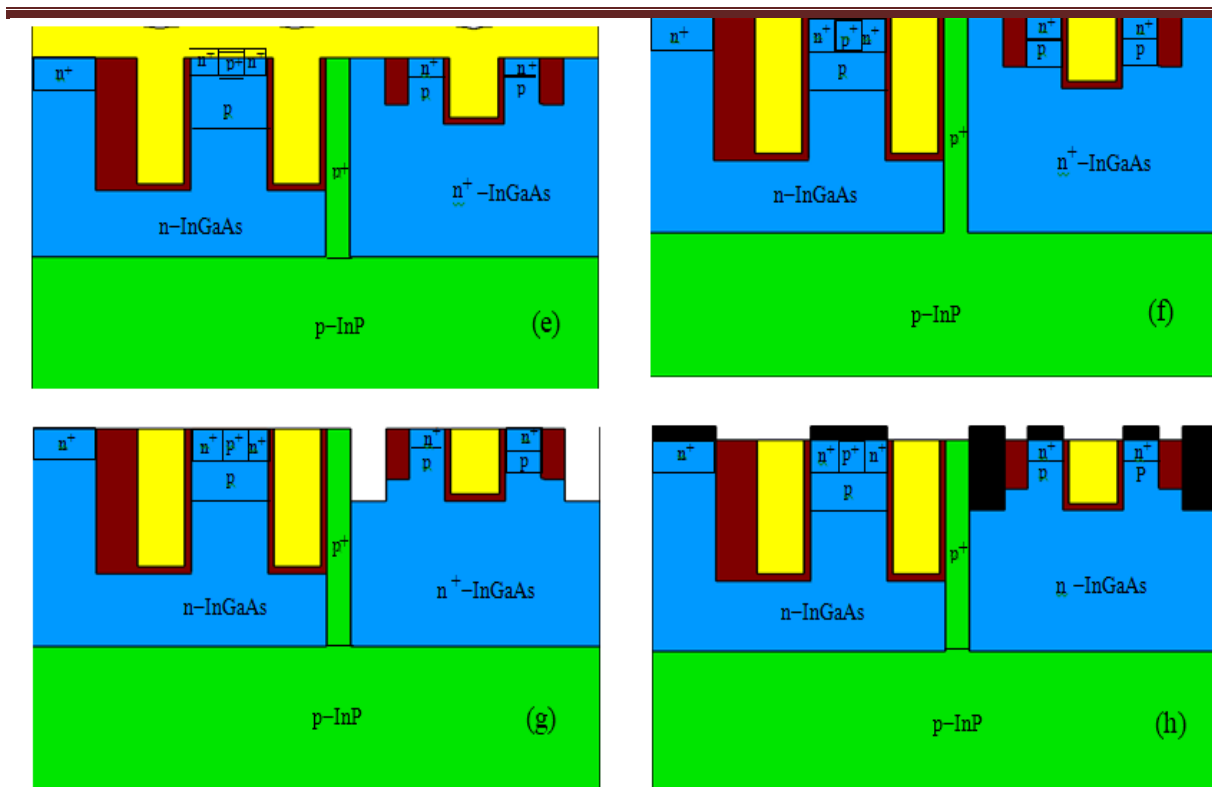


Figure 2: Construction Methods for Low Voltage MOSFETs and Junction-Isolated High Voltage DTG MOSFETs.

3. RESULTS&DISCUSSION

The SILVACO ATLAS software is used to do simulations of both high-voltage DTG MOSFETs and low-voltage MOSFETs with junction isolation, using either the CONMOB, Fermi-Dirac, FLDMOB, and CVT Lombardi models. At the InGaAs/ Al_2O_3 interface, we account for D_{it} by assigning it a value of $1 \times 10^{12} \text{ eV}^{-1} \text{ cm}^2$. The features of a high-voltage DTG MOSFET's output are shown in Fig.3 across a V_{GS} . At $V_{DS} = 15 \text{ V}$ and $V_{GS} = 2 \text{ V}$, the I_D of a high-voltage DTG MOSFET is $0.074 \text{ mA}/\mu\text{m}$. The figure shows the output features of a low-voltage MOSFET with a gate voltage of varied strengths when used with an LG of 60 nm. Channel formation in low-voltage MOSFET results in an I_D of $0.53 \text{ }\mu\text{A}/\text{m}$ at $V_{GS}=V_{DS}=1 \text{ V}$. High voltage DTG MOSFET transfer & transconductance characteristics are shown in Fig.4&5. At a constant current of $107 \text{ }\mu\text{A}/\mu\text{m}$, V_t is determined to be 1.32 V. The DTG MOSFET's high g_m is a result of the fact that both gates may manipulate the I_D at the same time. The gadget has a maximum g_m of $106 \text{ }\mu\text{S}/\mu\text{m}$ at a V_{GS} of 2.25 V.

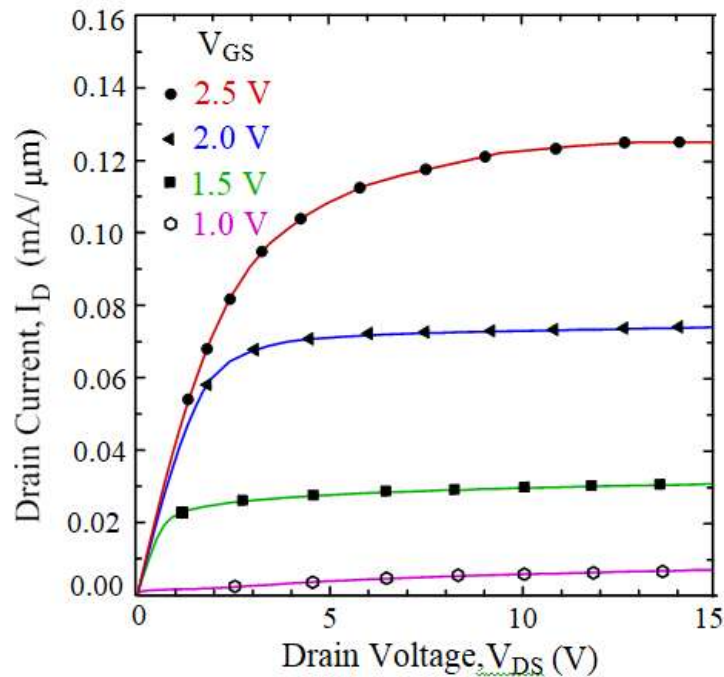


Figure3: High-voltage DTG MOSFET output characteristics.

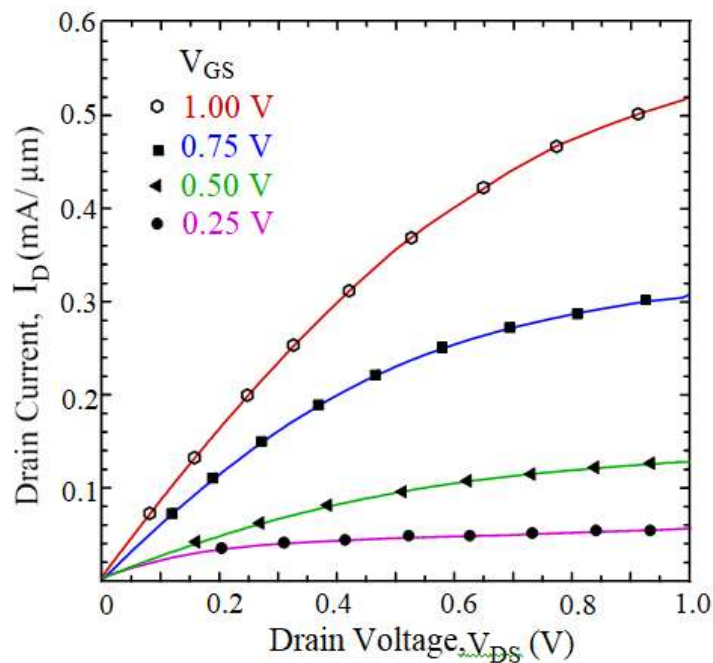


Figure 4: Features of the MOSFET's output at low voltage.

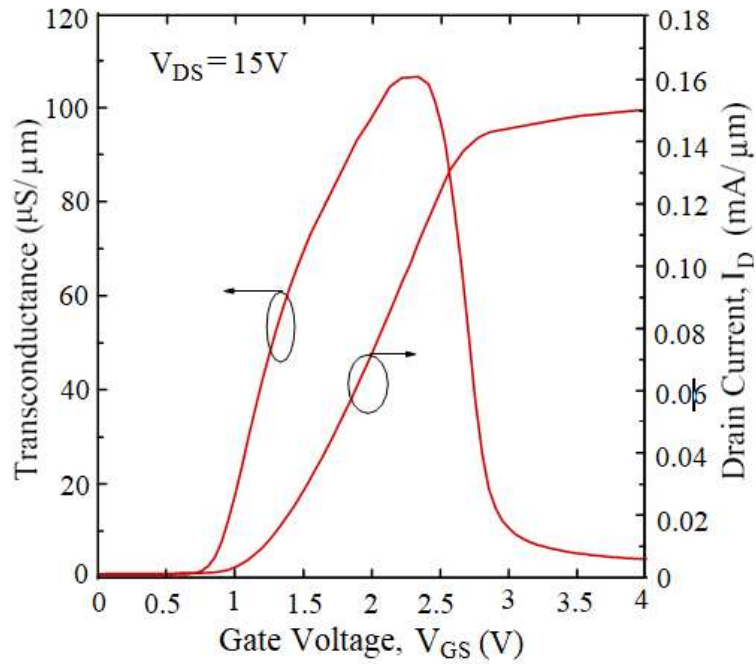


Figure 5: High voltage DTG MOSFET characteristics in terms of transfer and transconductance.

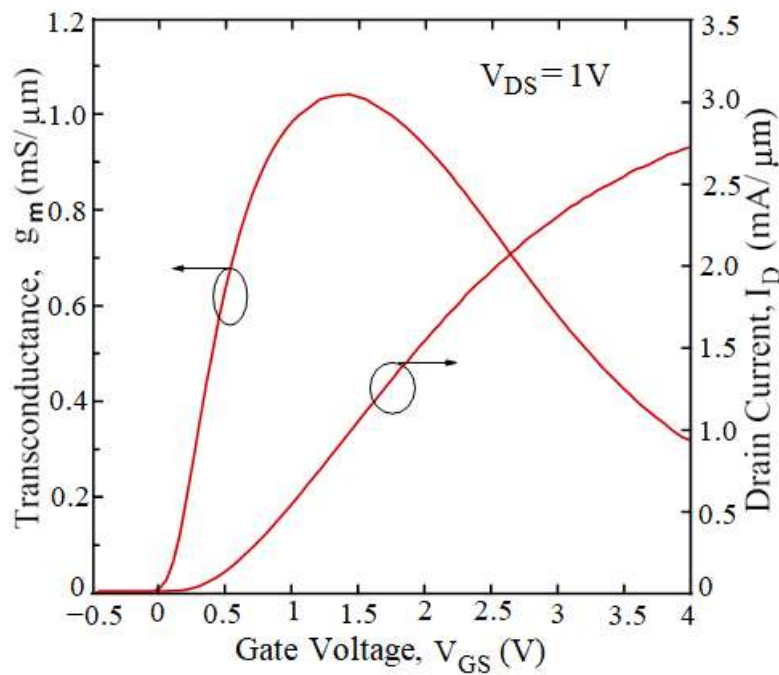


Figure 6: The low voltage MOSFET's transfer and transconductance properties.

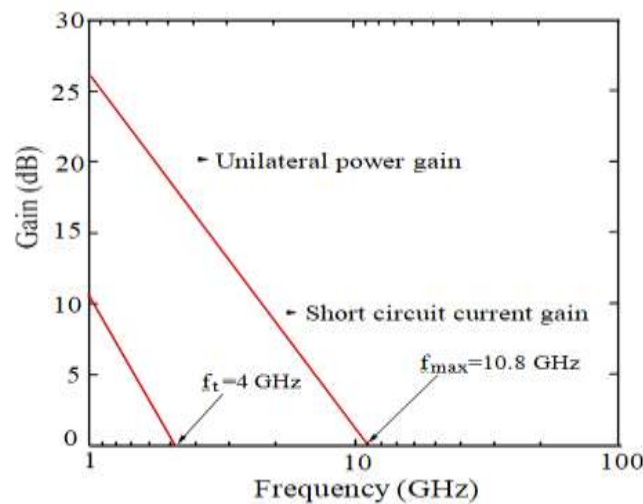


Figure 7: frequency dependence of the high-voltage DTG MOSFET's.

As can be seen in Fig.6 for a low voltage MOSFET, V_t equals 0.493 V, and max g_m is attained at 1.35 V for a gate-source voltage of 1.033 $\mu\text{mS}/\mu\text{m}$. Devices with a high g_m are well-suited for use as RF amplifiers. The DTG MOSFET's microwave properties are shown in Fig.7 Equipment's footing.

Whereas the highest frequency measured was 10.8 GHz. Capacitances at the gate and drain nodes were measured to be 0.6 fF/m and 8.08 fF/m, respectively.

The low voltage MOSFET's frequency characteristics are seen in Fig.8. The gadget has an f_t of 44 GHz when the current gain is at unity. The increased g_m of the MOSFET is responsible for the high value of f_t .

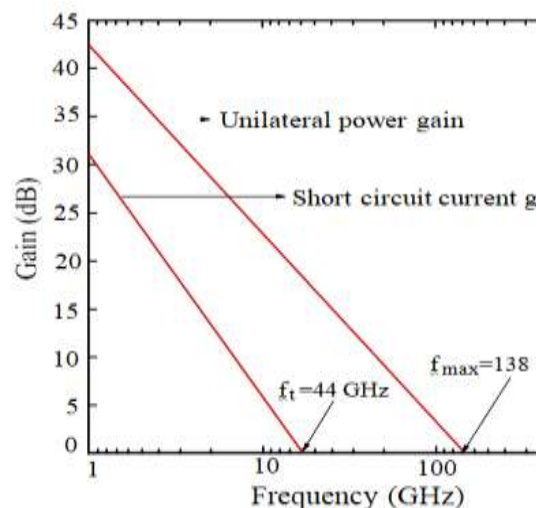


Figure 8: The low-voltage MOSFET's frequency response.

This low voltage MOSFET has a maximum frequency of 138 GHz. For the suggested MOSFET, the retrieved C_{gs} is 2.46 fF/ μm & the C_{gd} is 1.29 fF/ μm . In Fig.9, we see a plot of f_t and f_{max} vs V_{GS} for the low voltage MOSFET. At $V_{GS}=1.35$ V, the device's f_t and f_{max} are also at their highest.

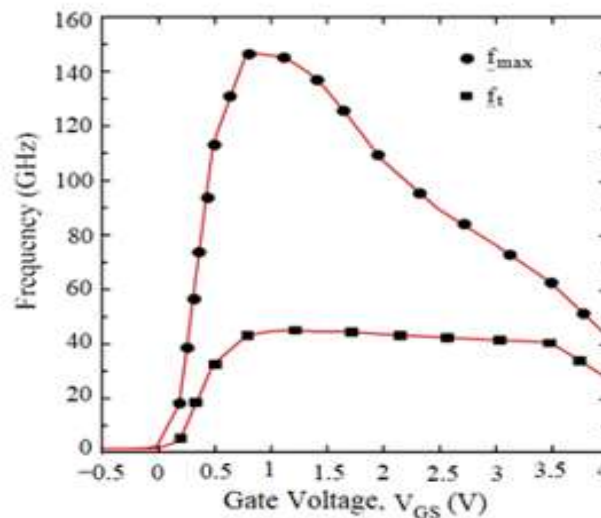


Figure 9: Changes in frequency with low-voltage MOSFET gate-source voltage

Sub-threshold behavior of the low-voltage MOSFET is seen in Fig.10. At $V_{DS}=1$ V, the structure's SS is 78 mV/dec for $LG=60$ nm. From this, we can determine that the MOSFET's DIBL is 118 mV/V. Small changes in V_t with V_{DS} , thanks to the trench gate's help in achieving greater control of the potential in the p-base, are responsible for the device's suppressed DIBL. Figure shows that at a V_{DS} of 1 V, the I_{ON} / I_{OFF} ratio of a low voltage MOSFET is 0.8×10^7 .

The high voltage DTG MOSFET's breakdown characteristics at $V_{GS}=0$ V are shown in Fig. 11. V_{br} is defined as the V_{DS} at which I_D is greater than 10×10^{12} A/ μm . The trench structure's high V_{br} of 52 V is attributed to the reduction of the electric field in the drift layer.

$R_{on, sp}$, and V_{br} for the high voltage DTG MOS- FET are shown to be N_d -dependent in Fig.12. Since the depletion layer covers the whole drift zone, the peak magnetic field within the device is reduced to 52 V for $N_d=1.5 \times 10^{16}$ cm^{-3} , as seen in Fig12. Due to the fact that the drain side of the drift region is not completely depleted, the number of field lines within the drift zone increases when $N_d > 1.5 \times 10^{16}$ cm^{-3} . Fig.13, demonstrates that when N_d increases, resistance within the drift zone decreases, leading to a decrease in $R_{on, sp}$.

The MOSFET offers the best compromise between V_{br} and $R_{on,sp}$. Fig. 13, Shows how $R_{on,sp}$ and V_{br} of the DTG MOSFET change as a function of t_d . Baliga's figure-of-merit is maximized for $t_d=1.5 \mu m$ using this gadget. Fig.14, displays the dependence of $R_{on,sp}$ on V_{GS} for the DTG MOSFET. The higher the V_{GS} , the more I_D there is, and hence the lower the $R_{on,sp}$. The $R_{on,sp}$ is calculated to be 51 mm^2 at a $V_{GS} = 10 \text{ V}$.

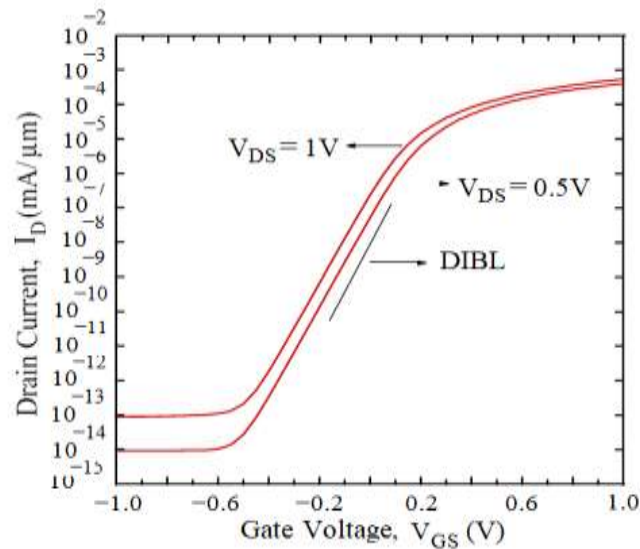


Figure 10: Typical low voltage MOSFET sub-threshold behavior.

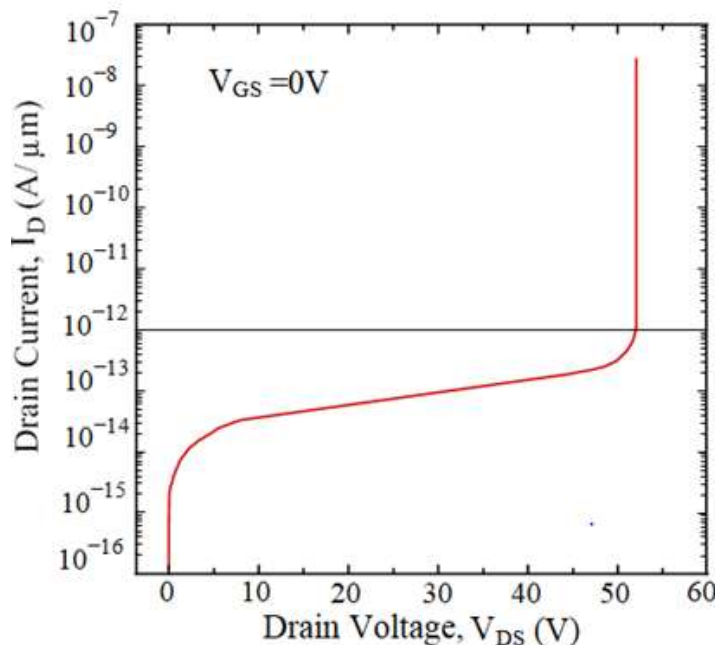


Figure 11: High voltage breakdown characteristics of a DTG MOSFET.

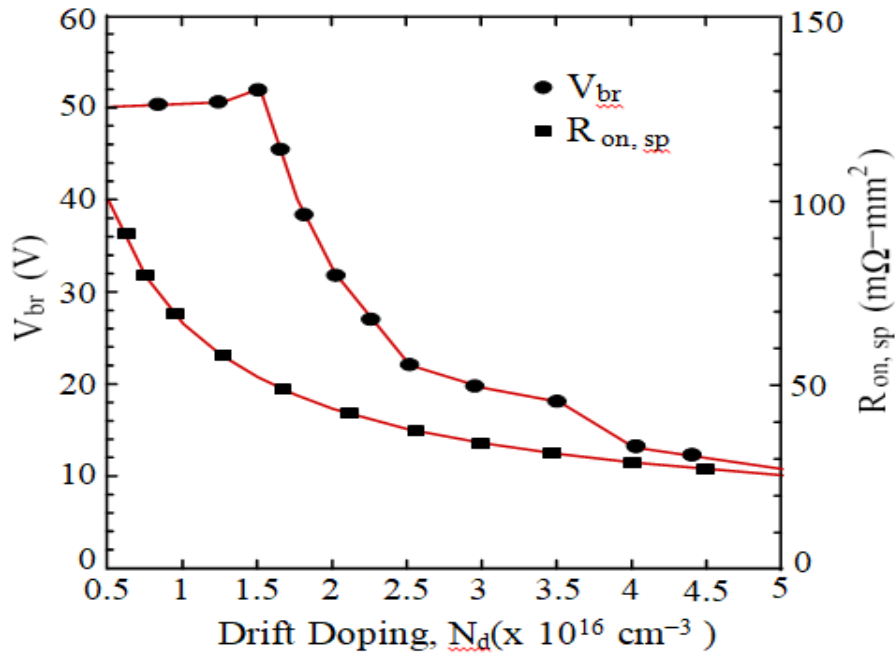


Figure 12: High-voltage DTG MOSFET V_{br} and $R_{on,sp}$ vs N_d .

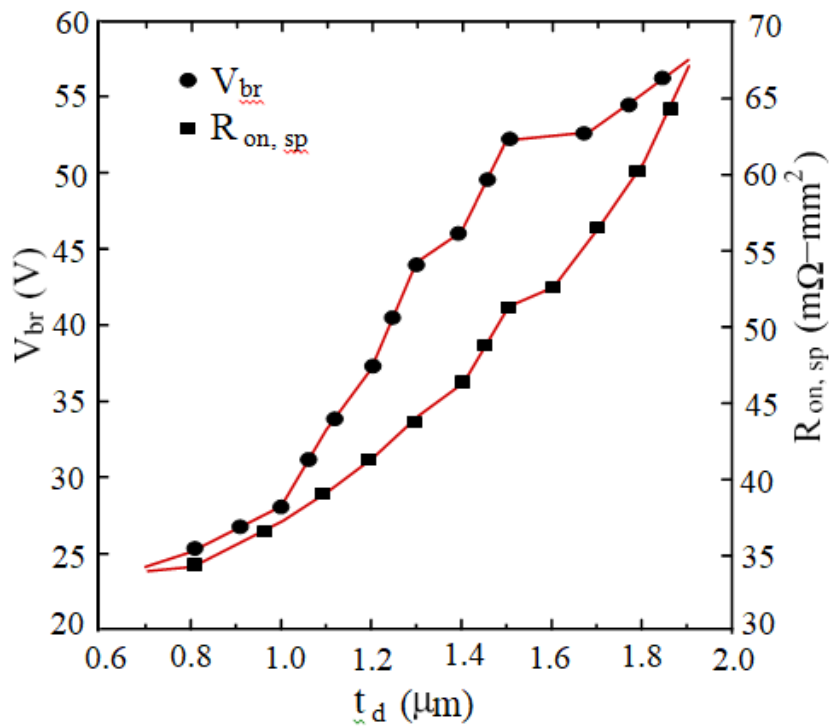


Figure 13: A plot of the high-voltage DTG MOSFET's V_{br} and $R_{on,sp}$ vs time-of-day.

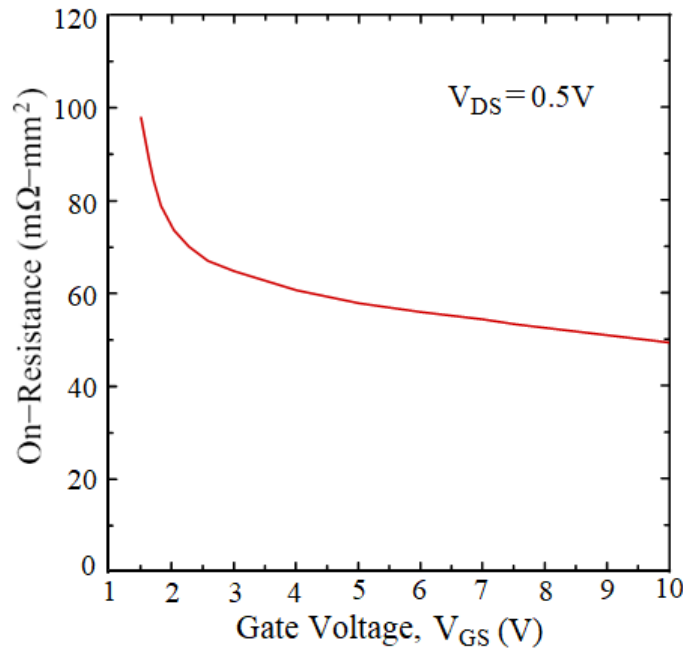


Figure 14: High voltage DTG MOSFET on resistance vs gate voltage.

4. CONCLUSION

In order to create smart power IC on InGaAs, it is suggested to combine high-voltage and low-voltage MOSFET architectures. Both devices' trench gates generate many p-base region channels, which increases I_D and decreases R_{on-sp} . By increasing the precision with which the gate electrodes are positioned across the I_D , f_t and f_{max} of the proposed devices may be enhanced. Two-dimensional simulations performed in a device simulator are used to evaluate the performance differences between a high-voltage DTG MOS-FET or a low-voltage small-signal MOSFET. It is shown that the static and dynamic properties of both devices are satisfactory. The suggested idea may be utilized to create digital and analog high-frequency power integrated circuits.



REFERENCES

1. K. Shenai, R. Branning, and J. Bokor, "High-voltage lateral MOSFETs in GaAs with controlled doping," *IEEE Transactions on Electron Devices*, vol. 39, no. 8, pp. 2017
2. Khurana, N. Shah, and D. K. Schroder, "A High Voltage n-Channel MOSFET in GaAs for Power Switching Applications," in *Proceedings of the IEEE International Electron Devices Meeting (IEDM)*, Washington, DC, USA, Dec. 2020, pp. 567-570.
3. P. Hazucha, L. K. Han, and P. M. Asbeck, "High voltage GaAs MESFET with a superjunction gate structure," *IEEE Transactions on Electron Devices*, vol. 44, no. 10, pp. 1797-1803, Oct. 2022.
4. S. H. Lee, Y. J. Kim, and J. K. Kim, "Low voltage GaAs MOSFET with a silicon nitride gate dielectric," *Solid-State Electronics*, vol. 45, no. 8, pp. 1355-1359, Aug. 2021.
5. Y. H. Lee, C. H. Lin, and J. R. Chen, "High-voltage lateral double-diffused MOSFET on GaAs substrate," *IEEE Electron Device Letters*, vol. 25, no. 1, pp. 5-7, Jan. 2018.
6. C. W. Chang and W. H. Chang, "Low-voltage GaAs MOSFET with an ultra-thin HfO₂ gate dielectric," *Solid-State Electronics*, vol. 49, no. 5, pp. 785-790, May 2015.
7. Y. S. Yang, S. H. Hsu, and C. K. Wang, "A high-voltage GaAs metal-oxide-semiconductor field-effect transistor with silicon nitride gate dielectric," *Journal of Vacuum Science and Technology B*, vol. 23, no. 5, pp. 1949-1952, Sep. 2015.
8. Y. H. Lee, C. H. Lin, and J. R. Chen, "High-voltage GaAs metal-oxide-semiconductor field-effect transistor with an Al₂O₃ gate dielectric," *IEEE Transactions on Electron Devices*, vol. 54, no. 10, pp. 2762-2766, Oct. 2017.
9. C. Li, Y. Li, and H. Li, "Low-voltage GaAs MOSFETs with thin LaAlO₃ gate dielectric," *Solid-State Electronics*, vol. 85, pp. 32-37, Aug. 2019.
10. J. Wu, Y. Jiang, and J. Shu, "A high-voltage GaAs MOSFET with an AlGa_N/Ga_Nsuperlattice gate dielectric," *IEEE Transactions on Electron Devices*, vol. 61, no. 10, pp. 3312-3316, Oct. 2015.